JOURNAL OF MATERIALS SCIENCE 26 (1991) 4803–4807

Investigation of crack closure in stainless steel by laser interferometry

Y. S. JO, S. I. KWUN
Department of Metallurgical Engineering, Korea University, Anam-dong, Sungbuk-ku, Seoul, Korea

The effect of strain-induced martensite transformed during fatigue on the fatigue crack propagation rate near ΔK_{th}, as well as low-cycle fatigue behaviour of three differently heat-treated stainless steels, was investigated. The heat treatments were chosen so that austenite stability during fatigue was different. The crack closure stress during fatigue crack propagation near the ΔK_{th} region was measured using laser interferometry. The sensitized specimen showed the highest value of closure load ratio (K_{cl}/K_{max}), which was considered to be due to the roughness-induced crack closure caused by intergranular facets. The specimen with the lowest austenite stability showing the largest amount of strain-induced martensite during fatigue, showed the highest crack growth rate. The effect of brittle fracture through the harder strain-induced martensite was larger than that of possible transformation-induced crack closure.

1. Introduction

It is well known that the fatigue crack growth is driven by the presence of a crack driving force, ΔK, and opposed by the resistance of crack-tip shielding or crack closure in the near threshold region [1–3]. Among several kinds of crack closure mechanisms, the phase transformation-induced crack closure [2–4] is somewhat rare.

Austenitic stainless steel shows strain-induced martensitic transformation with volume expansion [5, 6] upon plastic deformation, and fatigue damage can cause this kind of transformation below the martensitic deformation, M_d, temperature [7, 8]. Therefore, it is interesting to know whether the near-threshold fatigue crack growth rate of austenitic stainless steel might be affected by the phase transformation at room temperature. The microstructural change, such as carbide precipitation morphology, in austenitic stainless steel can enhance the strain-induced phase transformation near carbides due to lower Cr and C contents in this region [9]. When the regions around the grain boundaries become depleted in Cr and C, it will become more susceptible to strain-induced martensitic transformation. Upon deformation by fatigue, the initial transformation will occur in this region. Bearing the above points in mind, the AISI 304 austenitic stainless steel was used to study the crack closure phenomena in a material showing strain-induced phase transformation. Three different heat treatments, solution treatment, normal sensitization, and ageing at relatively high temperature were adopted to change the susceptibility to strain-induced martensitic transformation. Ageing at relatively high temperature for long times can lower the C and Cr contents more uniformly throughout the matrix than the normal sensitization treatment, and can also coarsen carbides. Thus the quantity of strain-induced martensite increases and the distribution becomes somewhat continuous throughout the matrix during fatigue in this heat treatment.

The near-threshold fatigue crack growth rate is very sensitive to microstructures [2, 3]. Therefore, it is expected that the above-mentioned heat treatments can vary the near-threshold fatigue crack growth behaviour by varying the amount of strain-induced martensites. The difference of near-threshold fatigue crack growth behaviour can be analysed by crack closure. There are several methods which can be used to measure crack closure. Foil strain gauge and clip gauge are the most widely used. In the case of microcracks, *in situ* detection with SEM has been performed by Morris and Buck [10] and the stereo-imaging technique [11] has also been used in some experiments. Recently, however, a new method with laser was tried to analyse the crack closure with great accuracy, and several successful experiments have been done by Sharpe and co-workers [12, 13]. In these experiments, the computer-aided laser interferometry system was used to determine the crack closure stress with high accuracy.

2. Materials and methods

The AISI 304 austenitic stainless steel (C 0.07, Si 0.64, Mn 1.05, P 0.03, S 0.007, Ni 8.51, Cr 18.12, N 0.034, Fe balance; wt %) was used in this study. The heat-treatment schedules employed for varying the carbide morphologies and thereby the austenite stability, together with their designations, are presented in Table I.

The annealed (ANN) condition showed no traces of carbides at all. The A10 condition (1050 °C, 30 min + water quench (WQ) + 650 °C, 10 h + WQ) shows the typical structure of grain-boundary sensitized

0022–2461/91 $03.00 + .12

TABLE I Heat-treatment conditions used

	Heat treatment
ANN	1050 °C, 30 min + WQ
A10	1050 °C, 30 min + WQ → 650 °C, 10 h + WQ
A60	1050 °C, 30 min + WQ → 700 °C, 60 h + AC

stainless steel, and the A60 condition (1050 °C, 30 min + WQ + 700 °C, 60 h + air cool (AC) shows the intra-grain carbides as well as grain-boundary carbides. The grain size was approximately 50 μm for each of the three conditions.

Specimens for low cycle fatigue tests were 3 mm thick plates with gauge length of 13 mm. The low-cycle fatigue tests were conducted at constant strain amplitudes of 0.5%, 0.7%, 0.9% and 1.1%. After low-cycle fatigue tests, the amount of strain-induced martensite transformed during fatigue was determined using ferrite scope and X-ray diffraction.

The 30 mm wide plate specimens for the fatigue crack propagation tests had initial 45° mechanical single notch of 3 mm depth. Fatigue crack propagation tests were conducted at a load ratio of $R = 0.05$ at room temperature. The frequency was 30 Hz and the wave shape was sinusoidal. The crack length was measured with a ×40 travelling microscope. The stress intensity range, ΔK, at the crack with a crack length, a, was calculated from [14].

$$\Delta K = 5\Delta P(\pi a)^{1/2}/(wt)[20 - 13(a/w) - 7(a/w)^2]^{-1/2} \quad (1)$$

where w is specimen width, t is specimen thickness and ΔP is load range. The fatigue threshold value, ΔK_{th}, was obtained by a load-shedding method [15], where ΔK_{th} was determined as the stress intensity range at $da/dN = 10^{-7}$ mm/cycle. Once ΔK_{th} was achieved, the load was raised slightly, and a K-increasing test was performed under constant load amplitude.

The crack closure load was determined by the laser interferometry method. With this method, the closure load was defined as the load corresponding to the initial deviation from linearity of the elastic compliance curve during unloading. The schematic view of the fringe pattern generation and recording system to get a compliance curve by the laser interferometry method is shown in Fig. 1. A shallow reflective indentation was impressed on either side of the crack using micro-Vicker's hardness tester. When a laser beam impinges upon the indentations, it is diffracted back at a particular angle with respect to the incident beam. The distance between the two indentations can be obtained from the relationship between the distance of the laser beam generator from the indentation and the interspacing of the fringe patterns. Fringe pattern intensity was sensed by a photo-TR in a box with a narrow slit mounted on the computer-controlled sliding stage. The current from the photo-TR was amplified and inputted into the computer through an A/D converter. The error in measuring the distances of fringes using this method was within 2%. To

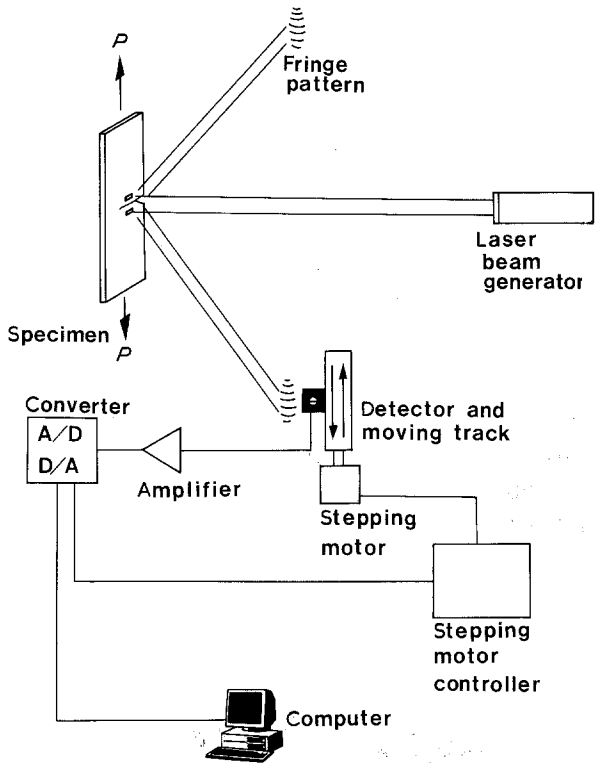

Figure 1 Schematic view of crack closure measurement apparatus.

study the effect of R on the crack closure stress, the fatigue crack propagation experiment was performed with R ratios of 0.5 and 0.05.

3. Results and discussion

Fig. 2 shows the fatigue crack growth rates of three different heat treatments in the low ΔK region. As can be seen, A10, the sensitized condition, shows the lowest crack growth rate while A60, the most unstable condition, shows the highest value. The ΔK_{th} values of these conditions were 15.2 and 6.91 MN m$^{-3/2}$, respectively. The ΔK_{th} value of ANN was 12.5 MN m$^{-3/2}$.

The fatigue crack growth rates in metals such as AISI 304 austenitic stainless steel, which show strain-induced phase transformation, are generally very low because of the high-energy absorbing capacity [16, 17]. However, it is not yet clear which is the main cause of the low rates of fatigue crack propagation of these materials, the high energy-absorbing capacity or the volume expansion in the plastic zone at the crack tip. In order to investigate the effect of strain-induced martensite at the crack tip on the fatigue crack propagation, the amount of transformed martensite was measured after low-cycle fatigue at several constant strain amplitudes. The amount of transformed martensite increased as the strain amplitude increased and the stability of austenite decreased, as shown in Table II. Also, as the strain amplitude increased, the rate of cyclic strain hardening increased in all three heat treatments, as shown in Fig. 3. This implies that the strain-induced martensites in austenitic stainless steel cause the strain hardening at the fatigue crack tip. The local areas along the grain boundaries in A10, and the relatively large areas inside the grains as well

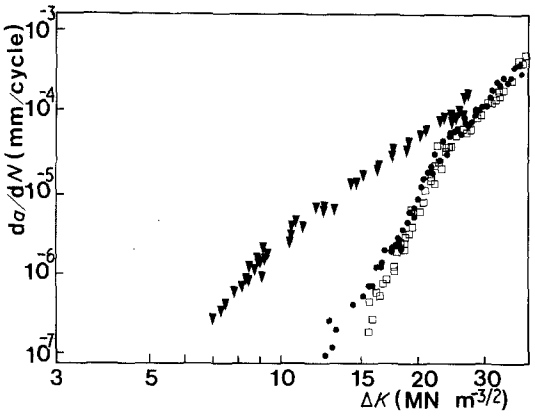

Figure 2 Fatigue crack growth rates of three different conditions in austenitic stainless steel. $R = 0.05$, (●) ANN, (□) A10, (▼) A60.

as along the grain boundaries in A60, might be easier for the transformation by fatigue damage than the matrix of ANN. It has been observed that the ΔK_{th} values decrease and the subsequent fatigue crack growth rate near the ΔK_{th} region increases with cyclic yield stress [18, 19]. It is believed that the strain-induced martensite is harder than austenite [20]. In general, the fatigue crack growth rate increases in the hardened area because of the lack of plasticity in the plastic zone. The presence of a large amount of transformed martensite in front of the propagating fatigue crack causing cyclic hardening is thought to increase the fatigue crack growth rate in A60, compared to the other two conditions.

That the A10 treatment which contains the strain-induced martensite along the grain boundaries by fatigue showed higher ΔK_{th} value than even ANN, requires more explanation. Table III shows the results of the crack closure test. A10 showed the highest K_{cl}/K_{max} values of the three conditions. The fatigue crack surface near ΔK_{th} of each condition (Fig. 4) shows rather quasi-cleavage-type fracture. However, the intergranular facets as shown in Fig. 5 were frequently observed in A10. The propagating fatigue crack might be retarded by the presence of the harder strain-induced martensites along grain boundaries. The Cr-carbides along grain boundaries are known to be the sites of crack initiation [21]. Therefore, the retarded crack at the grain boundaries reinitiate the fatigue crack and change the propagating direction at these areas into neighbouring grains. As a result, intergranular facets were formed at the grain boundaries in the A10 treatment resulting in a higher roughness-induced crack closure stress in the low ΔK region.

The load ratio produces a great effect on near-threshold fatigue crack growth rate. Fig. 6 shows the variation of crack growth rate characterized in terms of ΔK_{eff} and load ratio. In this experiment, the load ratios were 0.5 and 0.05. Studies of various steels [22–24] and non-ferrous alloys [25–27], tested at ambient temperature indicate that the values of ΔK_{th} decrease markedly and that crack propagation rates increase as the load ratio increases. In this study, the near-threshold crack growth rates increase with load

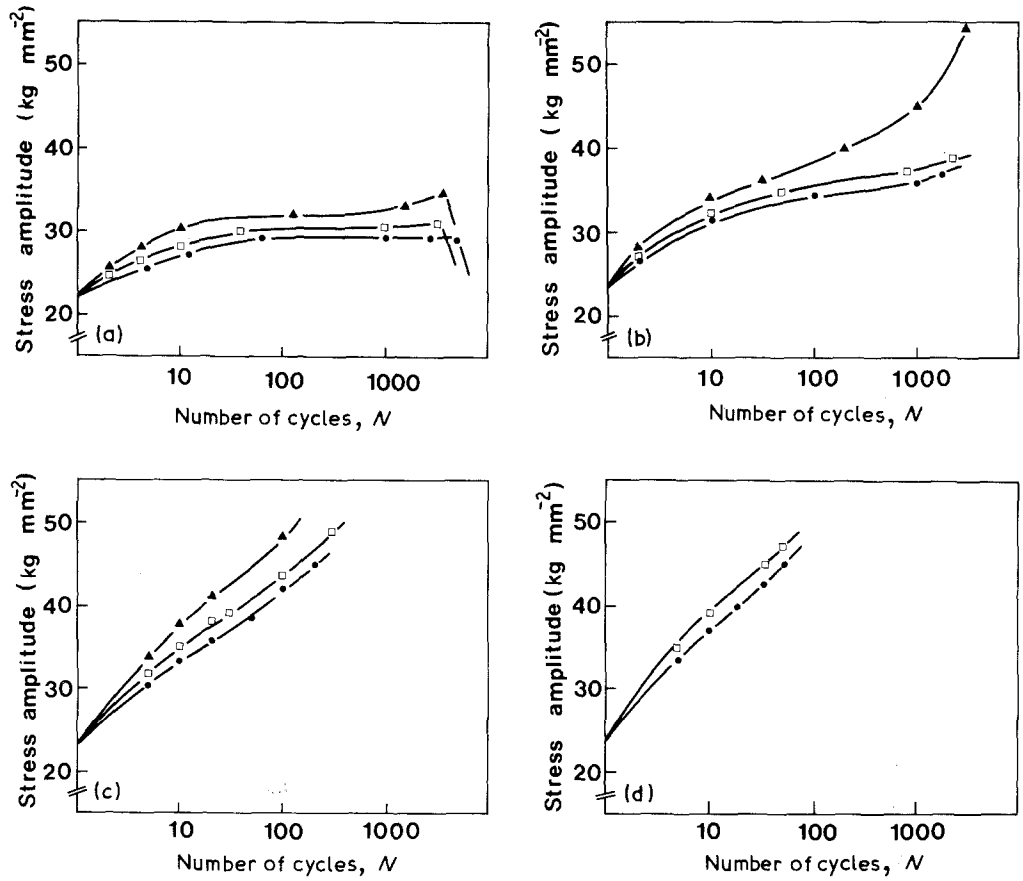

Figure 3 Stress response during low-cycle fatigue at different strain amplitudes. (a) $\Delta\varepsilon/2 = 0.5\%$, (b) $\Delta\varepsilon/2 = 0.7\%$, (c) $\Delta\varepsilon/2 = 0.9\%$ (d) $\Delta\varepsilon/2 = 1.1\%$. (▲) A60, (□) A10, (●) ANN.

TABLE II Volume percentage of strain-induced martensite in austenitic stainless steel after low-cycle fatigue

$\Delta\varepsilon/2$ (%)	ANN		A10		A60	
	Vol %	Number of cycles	Vol %	Number of cycles	Vol %	Number of cycles
0.5	1.25	5946	17	4110	34.8	5186
0.7	10.5	2055	19	1300	36.2	434
			27.5	1900		
0.9	8.5	130	36.2	434	38	130
	30.5	672			40.4	172

TABLE III K_{cl}/K_{max} values at different crack growth rates

ANN		A10		A60	
Crack growth rate (mm/cycle)	K_{cl}/K_{max}	Crack growth rate (mm/cycle)	K_{cl}/K_{max}	Crack growth rate (mm/cycle)	K_{cl}/K_{max}
5.2×10^{-7}	0.603	5.5×10^{-7}	0.676	3.0×10^{-7}	0.490
1.2×10^{-6}	0.508	9.5×10^{-7}	0.602	7.0×10^{-7}	0.406
2.0×10^{-6}	0.518	1.7×10^{-6}	0.478	1.4×10^{-6}	0.406
4.8×10^{-6}	0.500	2.2×10^{-6}	0.580	1.7×10^{-6}	0.360

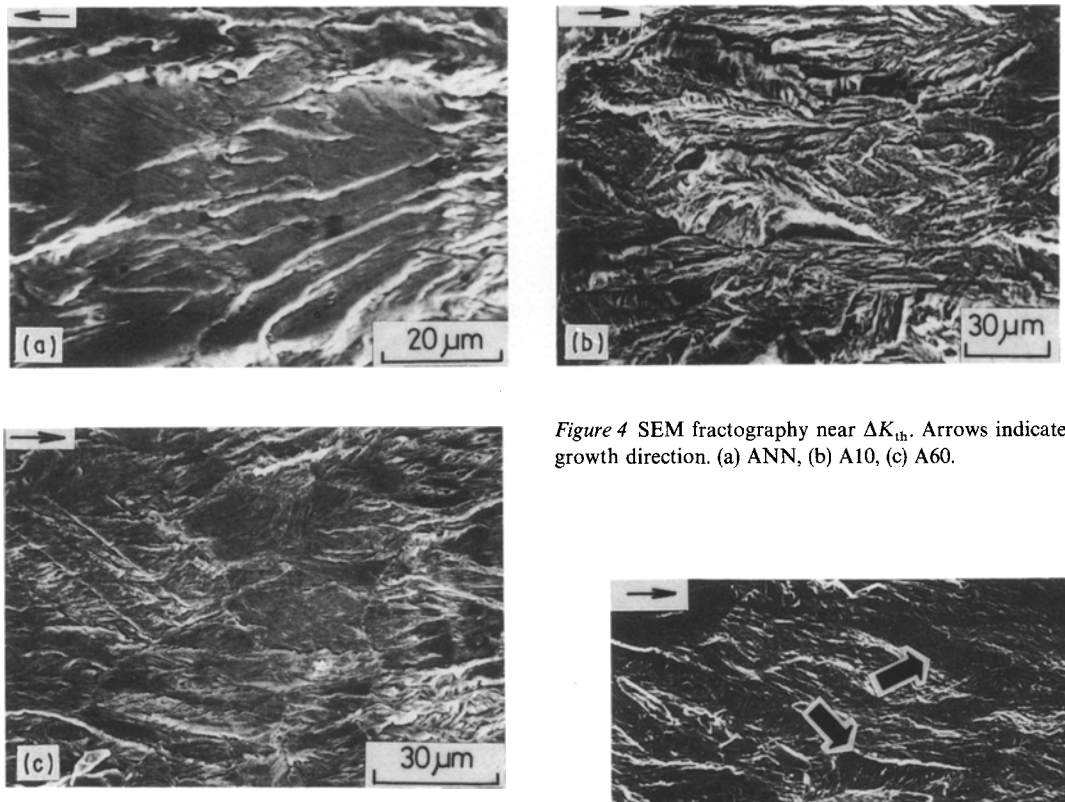

Figure 4 SEM fractography near ΔK_{th}. Arrows indicate the crack growth direction. (a) ANN, (b) A10, (c) A60.

Figure 5 SEM fractography showing the intergranular facets in A10 (45° tilted). →, crack growth direction; ➡, intergranular facet.

ratio. As can be seen in Fig. 6, the crack growth rates with $R = 0.5$ approach the crack growth rates characterized in terms of ΔK_{eff}. Because K_{cl}/K_{max} values lie between 0.5 and 0.6 in ANN and A10, the R ratio effect result seems reasonable. In general, an R ratio larger than K_{cl}/K_{max} may cause closure-free crack growth and this is true for ANN and A10. Despite a K_{cl}/K_{max} value lower than 0.5 in A60, the fatigue crack propagation rate at $R = 0.5$ was lower than that expected from the ΔK_{eff} versus da/dN plot. It is considered that the increase of mean load to $R = 0.5$ could not open the crack tip completely due to the relatively large transformation-induced compressive stress field in A60. However, the effect of this compressive stress on the fatigue crack propagation rate

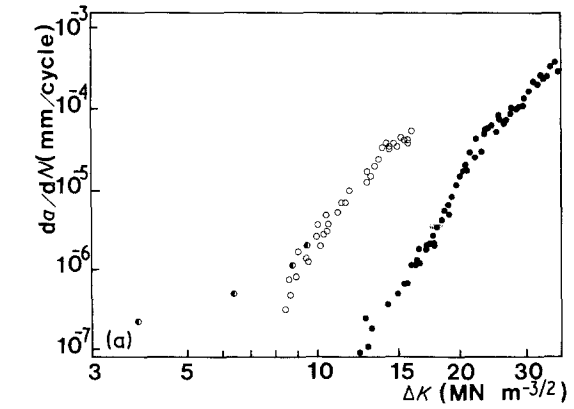

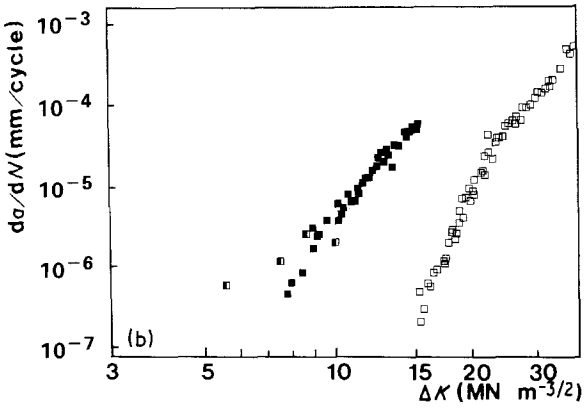

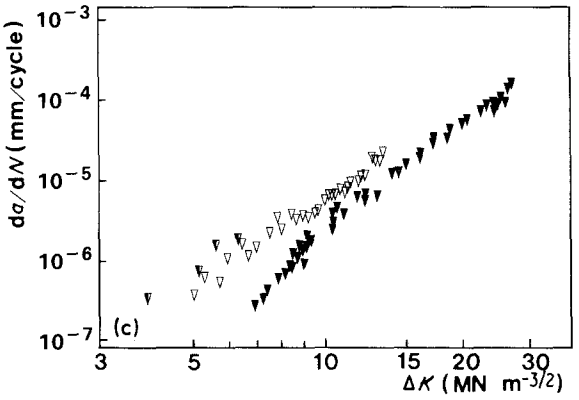

Figure 6 Fatigue crack growth rates at different load ratios. (a) ANN, (●) ΔK, $R = 0.05$, (○) ΔK, $R = 0.5$, (◐) ΔK_{eff}, $R = 0.05$; (b) A10, (□) ΔK, $R = 0.05$, (■) ΔK, $R = 0.5$, (◧) ΔK_{eff}, $R = 0.05$; (c) A60, (▼) ΔK, $R = 0.05$, (▽) ΔK, $R = 0.5$, (▼) ΔK_{eff}, $R = 0.05$.

seems to be lower than that of the rather flat quasi-cleavage fracture surface resulting in a lower roughness-induced crack closure.

4. Conclusions

1. The crack closure stress of the stainless steel was above 50% of the maximum stress at $R = 0.05$.

2. The sensitized condition showed the highest ΔK_{th} value. The strain-induced martensites along grain boundaries retard and deviate the propagating crack resulting in high roughness-induced crack closure.

3. The fatigue crack growth rate of the specimen with lowest austenite stability showed the highest value due to the cleavage fracture along relatively continuous martensites.

4. Strain-induced martensites, when homogeneously transformed throughout the matrix, retard the crack growth rate even at $R = 0.5$, because of the incomplete crack opening resulting from the residual compressive stress in the plastic zone at the crack tip.

5. The effect of R on the fatigue crack propagation rate could be predicted from the plot of da/dN versus ΔK_{eff} in this alloy.

Acknowledgement

The authors thank the Korea Research Foundation for financial support of this research.

References

1. JIAN KU SHANG, J.-L. TZOU and R. O. RITCHIE, *Metall. Trans.* **18A** (1987) 1613.
2. R. O. RITCHIE, W. W. GERBERICH and S. D. ANTOLOVICH, in "Mechanical Properties and Phase Transformation in Engineering Materials", TMS Annual Meeting in New Orleans, Louisianna, 26 March 1986, edited by S. D. Antolovich, R. O. Ritchie and W. W. Gerberich (Metallurgical Society, 1986) p. 59.
3. R. O. RITCHIE, in "Advances in Fracture Research", ICF6, Vol. 1, edited by S. R. Valluri (Pergamon, Oxford, 1984) p. 235.
4. J.-L. TZOU, S. SURESH and R. O. RITCHIE, *Acta Metall.* **33** (1985) 105.
5. S. S. HECKER, M. G. STOUT, K. P. STAUDHAMMER and J. L. SMITH, *Metall. Trans.* **13A** (1982) 619.
6. L. MURR, K. P. STAUDHAMMER and S. S. HECKER, *ibid.* **13A** (1982) 627.
7. D. HENNESSY, G. STECKEL and C. ALSTETTER, *ibid.* **7A** (1976) 415.
8. R. SHANANI and S. D. ANTOLOVICH, *ibid.* **5** (1974) 217.
9. C. L. BRIANT, in "Metallurgical Aspects of Environmental Failures", Vol. 12, edited by C. L. Briant (Elsevier Science, New York, 1985) p. 134.
10. W. L. MORRIS and O. BUCK, *Metall. Trans.* **8A** (1977) 597.
11. S. J. HUDAK Jr, *Trans. ASM* **103** (1981) 26.
12. W. N. SHARPE Jr, *Optic. Engng* **21** (1982) 482.
13. D. E. MACHA, W. N. SHARPE Jr and A. F. GRANDT Jr, "Crack and Fracture", ASTM STP601 (American Society for Testing and Materials, Philadelphia, Pennsylvania, 1976) p. 490.
14. L. P. POOK, *Int. J. Fract. Mech.* **4** (1968) 295.
15. R. J. BUCCI, ASTM STP738 (American Society for Testing and Materials, Philadelphia, PA, 1981) p. 5.
16. Y. S. JO and S. I. KWUN, *J. Korean Inst. Metals* **26** (1988) 62.
17. C. BATHIAS and R. M. PELLOUX, *Metall. Trans.* **4** (1973) 1265.
18. R. O. RITCHIE, *Met. Sci.* **11** (1977) 368.
19. *Idem, J. Engng Mater. Technol. (Trans. ASME, H)* **99** (1977) 307.
20. H. C. FIEDLER, B. L. AVERBACH and MORRIS COHEN, *Trans. ASM* **47** (1955) 267.
21. J. T. BARNBY and F. PEACE, *Acta Metall.* **19** (1971) 1351.
22. R. J. COOKE, P. E. IRVING, G. S. BOOTH and C. J. BEEVERS, *Engng Fract. Mech.* **7** (1975) 69.
23. P. E. IRVING and A. KURZFELD, *Met. Sci.* **12** (1978) 495.
24. P. K. LIAW and W. A. LOGSDON, *J. Engng Mater. Technol.* **107** (1985) 26.
25. J. PETIT and J. L. MAILLARD, *Scripta Metall.* **14** (1980) 163.
26. P. K. LIAW, T. R. LEAX, R. S. WILLIAMS and M. G. PECK, *Metall. Trans.* **13A** (1982) 1607.
27. P. E. IRVING and C. J. BEEVERS, *ibid.* **5** (1974) 391.

Received 2 January
and accepted 19 November 1990